Targeting of GFP to newborn rods by Nrl promoter and temporal expression profiling of flow-sorted photoreceptors

Masayuki Akimoto*†, Hong Cheng‡, Dongxiao Zhu§¶, Joseph A. Brzezinski‖, Ritu Khanna*, Elena Filippova*, Edwin C. T. Oh‡, Yuezhou Jing¶, Jose-Luis Linares*, Matthew Brooks*, Sepideh Zareparsi*, Alan J. Mears*,**, Alfred Hero§¶††‡‡, Tom Glaser‖§§, and Anand Swaroop*‡‖¶¶

Departments of *Ophthalmology and Visual Sciences, ¶Statistics, ‖Human Genetics, ††Electrical Engineering and Computer Science, ‡‡Biomedical Engineering, and §§Internal Medicine, Programs in ‡Neuroscience and §Bioinformatics, University of Michigan, Ann Arbor, MI 48105; †Translational Research Center, Kyoto University Hospital, Kyoto 606-8507, Japan; and **University of Ottawa Eye Institute and Ottawa Health Research Institute, Ottawa, ON, Canada K1H 8L6

Edited by Jeremy Nathans, Johns Hopkins University School of Medicine, Baltimore, MD, and approved January 6, 2006 (received for review September 20, 2005)

The Maf-family transcription factor Nrl is a key regulator of photoreceptor differentiation in mammals. Ablation of the *Nrl* gene in mice leads to functional cones at the expense of rods. We show that a 2.5-kb *Nrl* promoter segment directs the expression of enhanced GFP specifically to rod photoreceptors and the pineal gland of transgenic mice. GFP is detected shortly after terminal cell division, corresponding to the timing of rod genesis revealed by birthdating studies. In *Nrl*$^{-/-}$ retinas, the GFP+ photoreceptors express S-opsin, consistent with the transformation of rod precursors into cones. We report the gene profiles of freshly isolated flow-sorted GFP+ photoreceptors from wild-type and *Nrl*$^{-/-}$ retinas at five distinct developmental stages. Our results provide a framework for establishing gene regulatory networks that lead to mature functional photoreceptors from postmitotic precursors. Differentially expressed rod and cone genes are excellent candidates for retinopathies.

gene profiling | gene regulation | neuronal differentiation | retina | transcription factor

Evolution of higher-order sensory and behavioral functions in mammals is accompanied by increasingly complex regulation of gene expression (1). As much as 10% of the human genome is presumably dedicated to the control of transcription. Exquisitely timed expression of cell-type-specific genes, together with spatial and quantitative precision, depends on the interaction between transcriptional control machinery and extracellular signals (2, 3). Neuronal heterogeneity and functional diversity result from combinatorial and cooperative actions of regulatory proteins that form complicated yet precise transcriptional networks to generate unique gene expression profiles. A key transcription factor, combined with its cognate regulatory cis-sequence codes, specifies a particular node in the gene regulatory networks that guide differentiation and development (4).

The retina offers an ideal paradigm for investigating regulatory networks underlying neuronal differentiation. The genesis of six types of neurons and Müller glia in the vertebrate retina proceeds in a predictable sequence during development (5). Subsets of multipotent retinal neuroepithelial progenitors exit the cell cycle at specific time points and acquire a particular cell fate under the influence of intrinsic genetic program and extrinsic factors (5–7). Pioneering studies using thymidine labeling and retroviral vectors established the order and birthdates of neurons in developing retina (5, 8–10). The current model of retinal differentiation proposes that a heterogeneous pool of progenitors passes through states of competence, where it can generate a distinct subset of neurons (5). One can predict that, at the molecular level, this competence is acquired by combinatorial action of specific transcriptional regulatory proteins. Genetic ablation studies of transcription factors involved in early murine eye specification are consistent with combinatorial regulation (11–13).

Rod and cone photoreceptors account for 70–80% of all cells in the adult neural retina. In most mammals, rods greatly outnumber cones (95–97% of photoreceptors in mouse and human). Rods are born over a broad developmental window and, in mice, the majority are generated postnatally (5, 9, 14). Depending upon the time of their birth ("early" or "late"), postmitotic rod precursors exhibit variable delays before expressing the photopigment rhodopsin, a definitive marker of mature rods (6, 15–17). The molecular differences between early- and late-born rods and the mechanism(s) underlying the "delay" have not been elucidated. Nrl is a basic motif-leucine zipper transcription factor (18), which is specifically expressed in rod photoreceptors (19, 20) and pinealocytes (unpublished data). It interacts with cone rod homeobox (Crx), photoreceptor-specific orphan nuclear receptor (Nr2e3), and other proteins to regulate the expression of rod-specific genes (21–26). Missense mutations in the human *NRL* gene are associated with retinopathies (27, 28). Deletion of *Nrl* in mice results in a cone-only outer nuclear layer in the retina (29, 30), demonstrating its critical role in determining photoreceptor cell identity (29).

Based on its essential role in rod differentiation, we hypothesized that Nrl is the ideal transcription factor to gain insights into gene expression changes and regulatory networks underlying photoreceptor development. Here, using the Nrl-promoter to express GFP in transgenic mice, we show that Nrl is indeed the earliest rod lineage-specific marker. We directly demonstrate that the cells fated to become rods acquire a cone phenotype in the absence of *Nrl*, thereby establishing *Nrl* as the major cell-autonomous regulatory gene for rod differentiation. We also report gene profiles of GFP+ photoreceptors, isolated by FACS, from the wild-type and *Nrl*$^{-/-}$ retinas at five distinct stages of differentiation. These studies should assist in elucidating regulatory networks that lead to functional photoreceptors from postmitotic precursors.

Results and Discussion

Nrl Promoter Directs EGFP Expression to Rods. A comparison of the human and mouse Nrl promoter sequences identified four

Conflict of interest statement: No conflicts declared.

This paper was submitted directly (Track II) to the PNAS office.

Freely available online through the PNAS open access option.

Abbreviations: SOM, self-organizing map; E*n*, embryonic day *n*; P*n*, postnatal day *n*; wt, wild type; Nrl-ko-Gfp, *Nrl-L-EGFP:Nrl*$^{-/-}$; FDR-CI, false discovery rate confidence intervals.

Data deposition: The sequences reported in this paper have been deposited in the Gene Expression Omnibus database, www.ncbi.nlm.nih.gov/geo (accession no. GSE4051).

¶¶To whom correspondence should be addressed. E-mail: swaroop@umich.edu.

www.pnas.org/cgi/doi/10.1073/pnas.0508214103

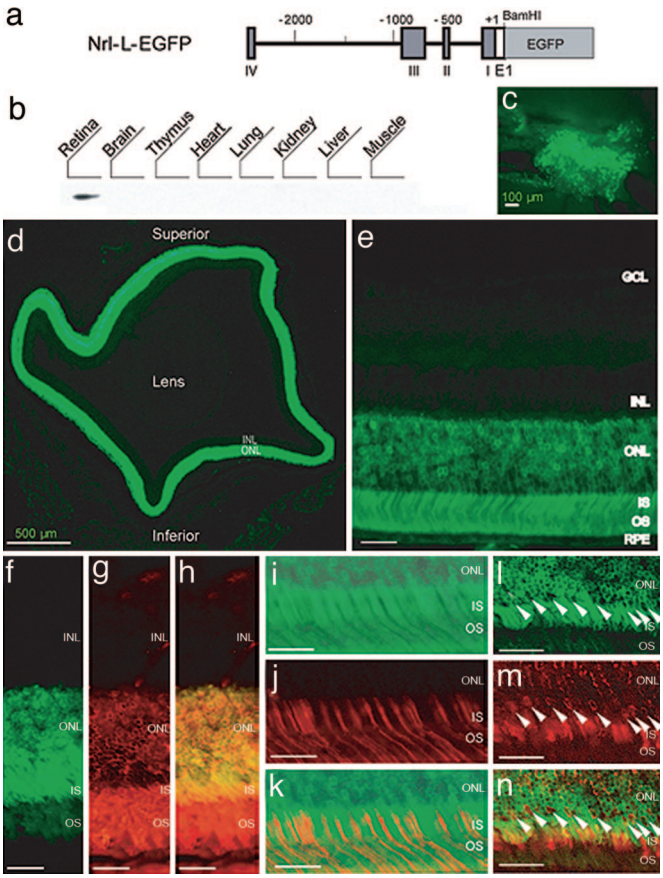

Fig. 1. Nrl promoter directs GFP expression to rods and pineal gland in transgenic mice. (*a*) Nrl-L-EGFP construct. The upstream Nrl segment contains four sequence regions I–IV that are conserved between mouse and human. E1 represents exon 1. (*b*) Immunoblot of tissue extracts (as indicated) using anti-GFP antibody, showing retina-specific expression of GFP in the Nrl-L-EGFP mouse. Transgenic mice generated with smaller constructs lacking one or more conserved promoter regions revealed aberrant or no expression of GFP (data not shown). (*c*) GFP expression in the pineal gland of Nrl-L-EGFP transgenic mice. (*d*) GFP expression in outer nuclear layer (ONL) of entire adult retina with (*e*) some nonfluorescent cells in the outer part of the ONL. (*f–h*) Immunostaining with rhodopsin antibody (red) showing a complete overlap with GFP (green) expression. (*i–k*) Cells positive for the cone-specific marker peanut agglutinin (red) do not overlap with GFP (green)-expressing cells. (*l–n*) Immunostaining with cone arrestin (red) reveals no overlap with GFP (green). Arrowheads indicate cone photoreceptor cells. As shown, GFP specifically labels the rod population in the retina. RPE, retinal pigment epithelium; OS, photoreceptor outer segments; IS, inner segments; ONL, outer nuclear layer; INL, inner nuclear layer; GCL, ganglion cell layer. [Scale bar, 100 μm (*c*), 500 μm (*d*), and 25 μm (*e–n*).]

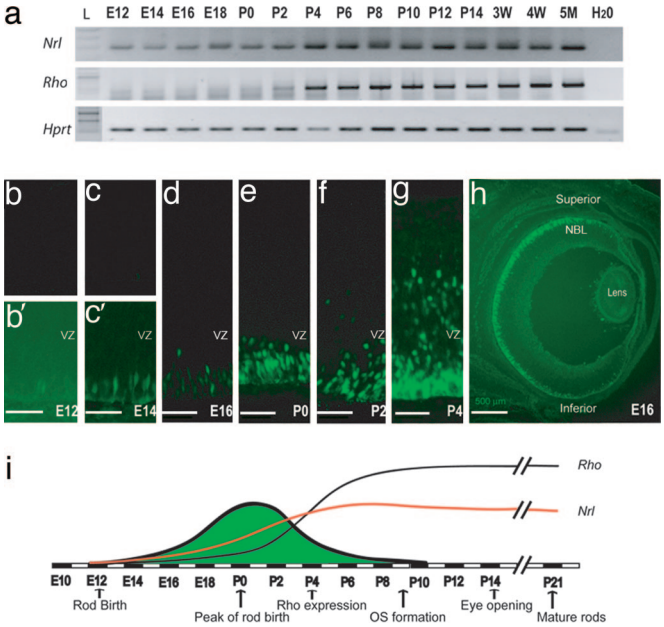

Fig. 2. The time course of GFP expression corresponds to rod cell birth in developing mouse retina. (*a*) RT-PCR analysis showing the expression of *Nrl* and *Rho* transcripts in developing and adult mouse retina, compared to an *Hprt* control. E and P indicate embryonic and postnatal day, respectively. W and M represent age in weeks and months, respectively. (*b*) GFP expression is first observed at E12 in a few cells with longer exposure (*b′*). (*c* and *c′*) Short and long exposures at E14, respectively. (*d–g*) Progressive increase in the intensity and number of GFP-expressing cells from E16 to P4. (*h*) Low-magnification view at E16 showing a dorsoventral gradient of GFP expression. (*i*) Timeline of rod photoreceptor birthdates (green area), major developmental events, and the kinetics of *Nrl* and rhodopsin (Rho) gene expression. VZ, ventricular zone; NBL, neuroblastic layer. [Scale bars, 25 μm (*b–g*) and 500 μm (*h*).]

conserved regions (designated I–IV) (Fig. 1*a*). The Nrl-L-EGFP construct, which included all four conserved regions (Fig. 1*a*), was used to generate transgenic mice. Six of the seven transgenic lines that we analyzed demonstrate GFP expression only in the retina (Fig. 1*b*) and pineal gland (Fig. 1*c*). In the adult retina, GFP is detected only in the outer nuclear layer, which contains rod and cone photoreceptor nuclei, and in the corresponding inner and outer segments (Fig. 1 *d* and *e*). Immunostaining with anti-rhodopsin antibody (15) shows complete colocalization with GFP (Fig. 1 *f–h*), whereas no overlap is observed between GFP and the cone-specific markers, peanut agglutinin (31) and cone arrestin (32) (Fig. 1 *i–n*). Hence, as predicted, all GFP-expressing cells are rod photoreceptors.

GFP Expression Corresponds to Rod Genesis in Developing Retina. In rodents, rods are born over an extended developmental period [embryonic day 12 (E12) to postnatal day 10 (P10)] overlapping with the birth of all neuronal subtypes in the retina (Fig. 2) (8, 9, 17). *Nrl* transcripts are detected by RT-PCR as early as E12 in mouse retina, considerably earlier than rhodopsin, which is expressed postnatally (Fig. 2*a*). To examine whether Nrl expression corresponds to rod genesis, we investigated GFP expression in developing retinas of the *Nrl-L-EGFP* mice [referred to as wild-type (wt)-Gfp]. The timing and kinetics of GFP expression in transgenic retinas, as revealed by RT-PCR, were consistent with early detection of *Nrl* transcripts (Fig. 7, which is published as supporting information on the PNAS web site). GFP-positive cells, although few and scattered, are first observed at E12 (Fig. 2 *b* and *b′*) and subsequently increase in abundance over time (Fig. 2 *c–h*). The spatial and temporal expression of GFP completely correlates with the timing and central-to-peripheral gradient of rod genesis, as previously indicated by [^{3}H]-thymidine birthdating experiments (Fig. 2*i*) (8, 9). No overlap was observed between GFP and the cell cycle markers Cyclin D1 and Ki67, which are expressed by cycling cells from late G_1 to M phase, and phosphohistone H3, which is expressed during M phase (Fig. 3 and Fig. 8, which is published as supporting information on the PNAS web site).

GFP Expression Is Detected in Rod Precursors Shortly After Terminal Mitosis. To further determine the onset of GFP expression in relation to the cell cycle, we performed short-term BrdUrd pulse–chase experiments in E16 embryos. Whereas GFP was not detected in BrdUrd-positive (S-phase) cells 1 h after the injection, we did observe double-labeled cells in embryos harvested at 4 and 6 h (Fig. 3), and their abundance increased at longer

NEUROSCIENCE

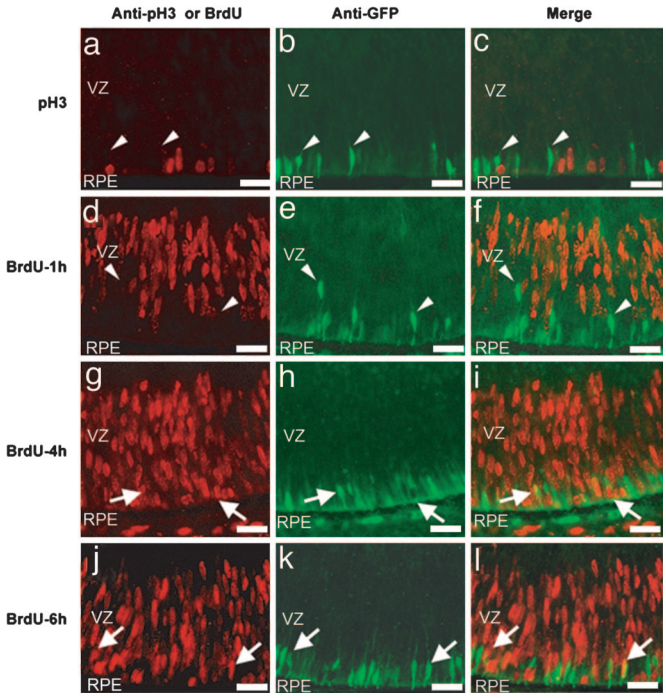

Fig. 3. GFP is expressed shortly after cell cycle exit. (*a–c*) E16 retinas from the wt-Gfp mice immunostained with antiphosphohistone H3 (pH3) (red) and anti-GFP (green) antibody. There is no colocalization, indicating that GFP+ cells are not in M-phase. (*d–l*) BrdUrd labeling experiments. (*d–f*) One hour after BrdUrd injection, no GFP+ cells (green, arrowheads) were labeled with BrdUrd (red), demonstrating that GFP+ cells are not in S-phase. (*g–i*) After 4 h, a small number of colabeled cells (arrows) were observed, indicating that GFP expression starts ≈4 h after the end of S-phase. (*j–l*) The number of colabeled cells increased 6 h after BrdUrd injection. VZ, ventricular zone; RPE, retinal pigment epithelium. (Scale bars, 10 μm.)

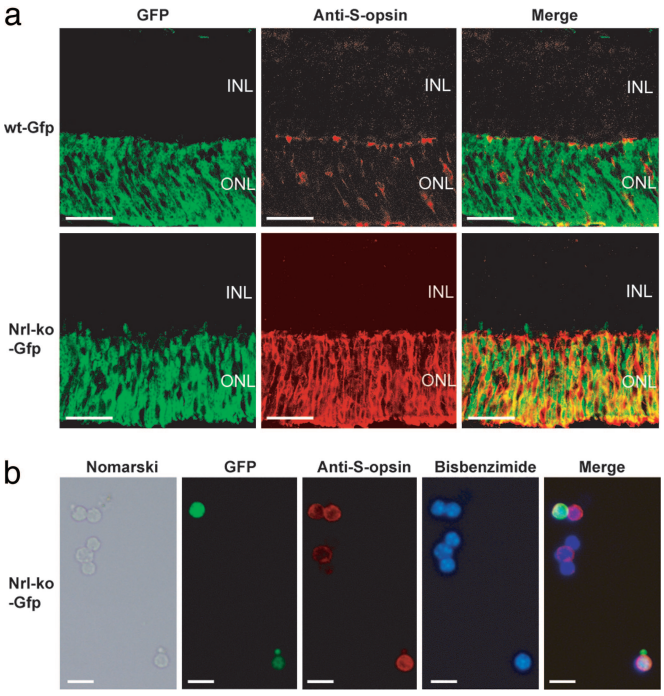

Fig. 4. GFP colocalizes with S-opsin in photoreceptors of the Nrl-ko-Gfp retina. (*a*) wt-Gfp and Nrl-ko-Gfp retinas (at P6) were immunostained with anti-S-opsin antibody. GFP and S-opsin are colocalized in the Nrl-ko-Gfp but not in the wt-Gfp mouse retina. (*b*) Dissociated cells from the P10 Nrl-ko-Gfp mouse retina were immunolabeled with S-opsin antibody. Bisbenzimide labels the nuclei. All GFP+ cells express S-opsin. However, ≈40% of S-opsin+ cones do not express GFP. This may reflect the loss of GFP during dissociation and immunostaining; decreased GFP expression in the absence of Nrl, which can activate its own promoter in mature rods (unpublished data); and/or contributions from the cohort of normal cones. Thus, GFP+ cells from the wt-Gfp and Nrl-ko-Gfp retina represent pure populations of rods and cones, respectively. [Scale bars, 50 μm (*a*) and 10 μm (*b*).]

intervals after BrdUrd exposure (data not shown). The durations of S and G_2 + M phases are estimated to be 10 and 4 h, respectively, in the E16 mouse retina (10, 33). Hence, our results imply that Nrl is expressed shortly after terminal division by cells that are fated to become rod photoreceptors, thereby establishing Nrl as the earliest known marker specific to rods. Additional support for these conclusions has been obtained by fate-mapping studies using cre-recombinase driven by the *Nrl* promoter (unpublished data).

Enhanced S-Cones in the Nrl$^{-/-}$ Retina Originate from Postmitotic Rod Precursors. The abundant S-cones in *Nrl*$^{-/-}$ mice are presumed to derive from rods that do not follow their appropriate developmental pathway due to the absence of Nrl (29). To directly evaluate the origin of enhanced S-cones in the *Nrl*$^{-/-}$ retina, we crossed the wt-Gfp mice with the *Nrl*$^{-/-}$ mice to generate *Nrl-L-EGFP:Nrl*$^{-/-}$ mice (referred to as Nrl-ko-Gfp). As shown in Fig. 4, the GFP+ cells (that are rod precursors in the wt retina) are colabeled with S-opsin in the Nrl-ko-Gfp retinas and in dissociated retinal cells from embryos and adults. Given that the S-opsin-expressing photoreceptors in the *Nrl*$^{-/-}$ retina are cones by morphological, molecular, and functional criteria (30), our data are consistent with the hypothesis that S-cones represent the "default fate" for photoreceptors (16, 34), at least in mice. We propose that *Nrl* determines the rod fate within "bipotent" photoreceptor precursors by modulating gene networks that simultaneously activate rod- and suppress cone-specific genes.

Gene Profiling of Purified GFP+ Photoreceptors Reveals Specific Regulatory Molecules Associated with Terminal Differentiation. To elucidate the genes and regulatory networks associated with differentiation of photoreceptors from committed postmitotic precursors, we performed genome-wide expression profiling of GFP+ cells purified from the retinas of wt-Gfp and Nrl-ko-Gfp mice at five distinct developmental time points (E16, P2, P6, P10, and P28) (Figs. 9 and 10, which are published as supporting information on the PNAS web site). Given that rods are born over a relatively long period of retinal development (E13–P10), GFP+ cells from wt-Gfp retinas at any specific time will represent rods at discrete stages of differentiation; nonetheless, profiles from GFP+ cells at E16 and P2 will broadly reflect genes expressed in early- and late-born rods, respectively. The profiles of GFP+ cells purified at P10 and P28 are expected to reveal many genes involved in outer segment formation and phototransduction, respectively. From the GeneChip data, we first generated a bitmap of present/absent calls for all probesets at the five developmental stages from wt-Gfp mice (Fig. 5*a*); this diagram indicates the proportion of genes found to fit in any one of 32 potential present/absent patterns and includes gene signatures for each time point. Together with a similar bitmap for Nrl-ko-Gfp (not shown), these data reveal expression of ≈20,000 transcripts in photoreceptors, consistent with previous retinal transcriptome estimates (35). We then generated independent ranked lists of the top 1,000 genes that are differentially expressed across developmental stages for both wt-Gfp and Nrl-ko-Gfp retinas; each of these genes has a false discovery rate confidence interval (FDR-CI) P value ≤ 0.15 and true fold change ≥ 2 in at least one pair of time points. Significantly more genes were differentially expressed over time in these FACS-purified cells

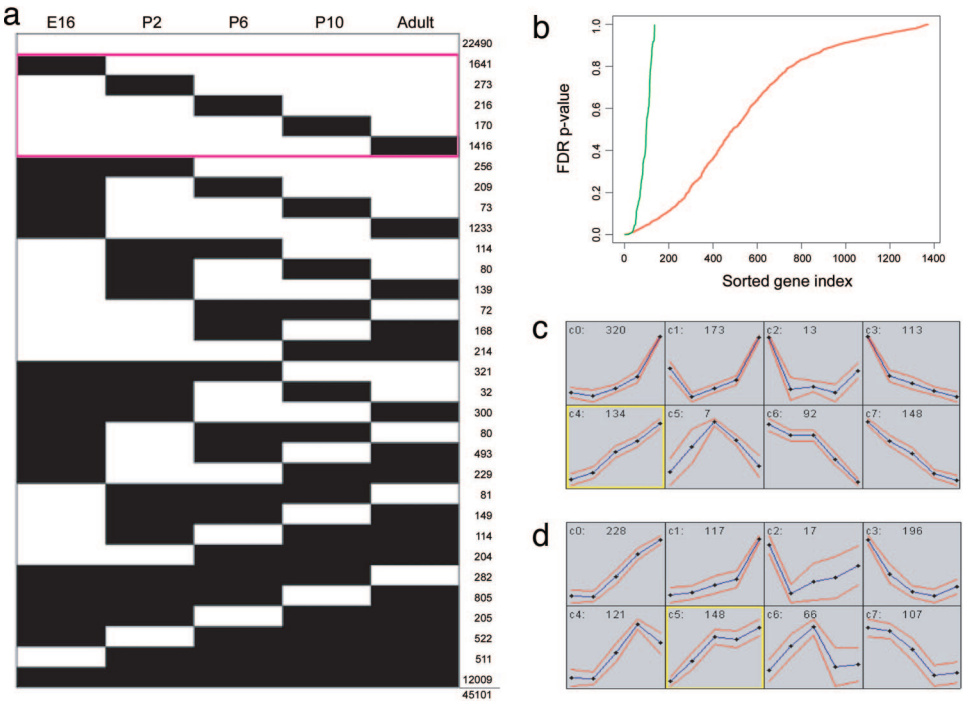

Fig. 5. Gene profiles of FACS-purified GFP+ photoreceptors reveal unique differentially expressed genes and significant advantages over whole retina analysis. (*a*) Bitmap for gene expressions. The 45,101 probesets were determined as present (black) or absent (white) at each of five developmental stages; all genes were assigned to one of the $2^5 = 32$ possible expression clusters, which are represented by black/white patterns and correspond to 32 rows in the bitmap. The bitmap of gene expression profiles for wild-type developing rods is shown, with the number of genes in each cluster indicated. The boxed clusters represent molecular signatures for each developmental stage. A similar bitmap was generated for developing cones from the Nrl-ko-Gfp retina (not shown). (*b*) Comparison of gene profiling data from FACS-purified photoreceptors (reported here) with those from the whole retina (26). The two data sets (red from this report and green from ref. 26) were analyzed by using FDR-CI with 2-fold maximum acceptable difference (MAD) constraint. The horizontal axis represents the sorted gene index according to FDR *P* values, and the vertical axis represents FDR *P* values. At similar FDR *P* values, >10 times more differentially expressed genes are extracted in the profiling data reported here compared to Yoshida *et al.* (26), thereby allowing for much stronger discovery power. (*c*) SOM clustering of selected wt (wt-Gfp) gene expression profiles. Clusters of top 1,000 differentially expressed genes over five developmental stages were projected onto a 2D 2 × 4 grid. These were selected empirically, for maximal changes in expression levels over time, to capture biologically nonredundant patterns of interest. Within each image, expression levels are shown on *y* axis and the five developmental stages (in *a*) are shown on *x* axis from left to right (from earliest to latest). The middle curve (blue) is the mean expression profile of genes in that cluster, and the upper/lower curves (red) show the standard deviation (±). The cluster index (c#) and the number of genes in each cluster are indicated. The cluster containing rhodopsin (highlighted in yellow) includes genes whose expression increases progressively as photoreceptors mature, from P6 to adult. (*d*) SOM clustering of selected $Nrl^{-/-}$ (Nrl-ko-Gfp) gene expression profiles. The details are essentially the same as in *c*. The cluster containing S-cone opsin and genes involved in cone maturation is highlighted in yellow.

(Fig. 5*b*) than were identified in comparable gene profiles of the whole retina (26). Self-organizing map (SOM) clusters were then derived from wt-Gfp and Nrl-ko-Gfp gene profiles, as described (36). Interestingly, similar clusters in the two profiles reveal major differences, which in large part correspond to distinctions between rods and cones (Fig. 5 *c* and *d*). Predictably, the clusters that include rhodopsin (cluster 4 in wt-Gfp, Fig. 5*c*) or S-opsin (cluster 5 in Nrl-ko-Gfp, Fig. 5*d*) exhibit a significant increase in expression at P10 and P28 (Tables 1 and 2, which are published as supporting information on the PNAS web site). Together with a whole retina microarray, serial analysis of gene expression, and *in situ* hybridization studies (26, 35, 37–39), our gene profiles will facilitate rapid discovery of genetic defects in photoreceptor diseases.

To obtain insights into the delay (16, 17) associated with the expression of phototransduction genes, we compared the gene profiles of E16, P2, and P6 photoreceptors (Table 3, which is published as supporting information on the PNAS web site); 25 of 34 differentially expressed genes could be validated by real-time PCR (Fig. 11*a*, which is published as supporting information on the PNAS web site). As predicted, at P6, we observe high expression of genes involved in photoreceptor integrity and function (such as *Rho*, *Pde6b*, *Rs1h*, *Rp1h*, *Rdh12*, and *Rpgr*). We also detect altered expression of a battery of regulatory factors at P6 when compared to the profiles at E16 or P2. Several of the genes display decreased expression as the differentiation proceeds and are either antidifferentiation factors (e.g., *Id2*) or negative regulators ("the brake genes") of rod maturation. Likewise, the regulatory genes showing higher expression at P6 (*Bteb1* and *Jarid2*) are candidate coactivators of rod differentiation.

Cluster Analysis of Gene Profiles from the GFP-Tagged wt and $Nrl^{-/-}$ Photoreceptors Identifies Expression Differences Between Rods and Cones. We then compared wt-Gfp and Nrl-ko-Gfp data; heat maps of the top 1,000 differentially expressed genes selected over five developmental stages reveal several expression clusters; two of the clusters shown here reveal the genes whose expression increases (cluster I) or decreases (cluster II) with time in Nrl-ko-Gfp cells (Fig. 6). Although cluster II includes a number of well characterized rod-specific genes (such as *Nrl*, *Nr2e3*, *Rho*, and *Pde6b*), cluster I has several genes that are predicted to be involved in cone function. Real-time PCR analysis of 19 differentially expressed genes demonstrated complete to partial concordance with microarray data for 15 genes over five developmental stages in both wt-Gfp and Nrl-ko-Gfp cells (Fig. 11). We cannot, however, rule out that some expression changes in Nrl-ko-Gfp cells are due, at least in part, to structural aberrations or stress response noted in these fate-switched photoreceptors (29, 30, 40). Genes that are differentially expressed during development and between wt-Gfp and Nrl-ko-Gfp photoreceptors are attractive targets for functional studies and as candidates for retinal dystrophies (see Tables 1 and 2).

Conclusion

In this report, we provide a direct demonstration of the temporal and spatial genetic identity of a differentiating neuron (rod photoreceptor) in mammals. We show that Nrl (as accurately recapitulated by the GFP reporter) is the earliest specific marker of postmitotic rod precursors. The functionality of Nrl promoter in the developing $Nrl^{-/-}$ retina (similar to that in wt retina) suggests the availability of signaling factors for rod determination, yet the GFP-tagged rod precursors acquire the identity of S-cones when *Nrl* is absent. This implies the existence of pool(s)

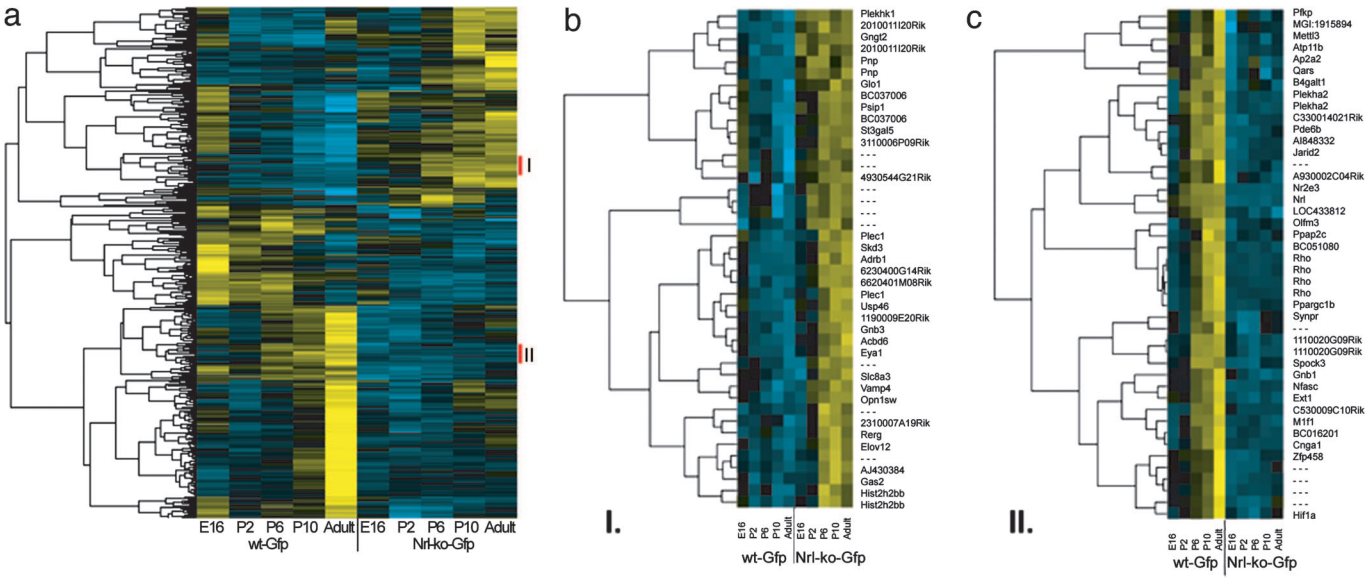

Fig. 6. Cluster analysis of differentially expressed genes. (*a*) Hierarchical clustering of top 1,000 differentially expressed genes across wt, Nrl-ko, and five developmental stages, selected by two-stage filtering. Bright blue boxes indicate lowest signal with increasing values indicated by darkening color toward bright yellow, representing peak signal. (*b*) Cluster I includes genes that exhibit increased expression during cone development and show dramatically increased expression in the $Nrl^{-/-}$ photoreceptors, such as *Opn1sw* (S-cone opsin), *Gnb3* (cone transducin), and *Elovl2* (long-chain fatty acid synthase). (*c*) Cluster II includes genes that exhibit increased expression during rod development and show dramatically reduced expression in the cones, such as *Rho* (rhodopsin), *Nr2e3* (nuclear receptor, mutated in *rd7* mice), *Pde6b* (rod GMP phosphodiesterase 6B, mutated in *rd1* mice), and *Nrl*.

of progenitor cells with competence to become either a rod or a cone (i.e., binary cell fate choice) (29) at an earlier step in retinal development. We propose that, during early stages of development, postmitotic precursor cells are not completely committed to a specific photoreceptor fate (i.e., are plastic) and transcriptional regulators, such as *Nrl* (29) or *Trb2* (41), instruct these cells to produce rods or M-cones, respectively. It is possible that S-cones represent the ''default'' state or require another as-yet-unidentified activator for differentiation. These results are consistent with evolutionary data suggesting that rods are derived from an ancestral cone(s) (42–44).

We have applied genome-wide profiling to investigate expression dynamics of specific neurons developing within a single lineage over time, from commitment to maturation, using purified cell populations. Our data provide a comprehensive view of genetic determinants that specify rod and cone morphology and function. We expect that wt-Gfp transgenic mice will be valuable for investigating progenitor plasticity, determining the precise role of individual genetic mutations on rod and cone differentiation or function, and evaluating cellular treatment paradigms for retinal and macular degeneration.

Materials and Methods

Comparison of 5′-Upstream Sequences of the Human and Mouse *Nrl* Genes. We isolated and sequenced a mouse *Nrl* genomic clone from a 129 × 1/SvJ-derived Lambda Fix II genomic library (Stratagene). Genomic sequences 3 kb upstream of the human *NRL* (AL136295) and mouse *Nrl* transcription start sites (AY526079) were compared by BLAST2 (www.ebi.ac.uk/blastall/vectors.html).

Plasmid Constructs and Generation of Transgenic Mice. A 2.5-kb upstream segment of the mouse *Nrl* gene (from −2408 to +115) was cloned into the pEGFP1 vector (Clontech) (Nrl-L-EGFP construct; Fig. 1*a*). The 3.5-kb insert from Nrl-L-EGFP, excluding the vector backbone, was injected into fertilized (C57BL/6 × SJL) F_2 mouse oocytes, which were implanted into pseudopregnant females (University of Michigan transgenic core facility). Transgenic founder mice and their progeny were identified by PCR, and transgene copy number was estimated by Southern blot analysis of tail DNA using an EGFP gene probe. The founders were bred to C57BL/6 mice to generate F_1 progeny. A mouse line with three copies of the transgene was used for subsequent studies.

Immunoblotting and Immunostaining. The detailed methods have been described (19, 29). For immunoblot analysis, the primary antibodies were rabbit anti-GFP pAb (Santa Cruz Biotechnology) or mouse anti-GFP mAb (Covance Research Products, Cumberland, VA). For immunofluorescence, we used 10-μm retinal cryosections or retinal cells isolated with papain dissociation system (Worthington). Primary antibodies were: GFP, rabbit pAb (Upstate Biotechnology, Lake Placid, NY) or rabbit pAb conjugated to Alexa Fluor-488 (Molecular Probes); rhodopsin, mouse mAb (Rho4D2, kind gift of R. Molday, University of British Columbia, Vancouver); cone arrestin, rabbit pAb (kind gift of C. Craft, University of Southern California, Los Angeles); phosphohistone H3, rabbit pAb (Upstate Biotechnology); Cyclin D1, mouse mAb (Zymed); Ki67, mouse mAb (DAKO); BrdUrd, rat mAb (Harlan Sera-Lab, Loughborough, U.K.). Texas red-conjugated peanut agglutinin lectin (PNA) was obtained from Vector Laboratories. Fluorescent detection was performed by using Alexa Fluor-488 or -546 (Molecular Probes) and FITC or Texas red (Jackson ImmunoResearch)-conjugated secondary antibodies. Sections were visualized under a conventional fluorescent microscope and digitized.

BrdUrd Staining. Pregnant females were given single i.p. injection of BrdUrd (Sigma, 0.1 mg/g body weight) on E16. Embryos were dissected 1, 4, 6, or 12 h after injection, fixed in 4% paraformaldehyde, and cryosectioned. Immunostaining was performed sequentially to detect GFP and then BrdUrd. After GFP immunostaining with primary and secondary reagents, sections were washed in PBTx (PBS + 0.1% Triton X-100) and incubated in 2.4 M HCl/PBTx for 75 min. Sections were then washed and immunostained for BrdUrd.

RNA Preparation and Real-Time PCR. Total RNA was extracted by using TRIzol (Invitrogen) and treated with RNase-free DNase I

before reverse transcription. Quantitative real-time PCR was performed with iCycler IQ system (Bio-Rad).

FACS Enrichment and Microarray Hybridization. Mouse retinas were dissected at five time points: E16, P2, P6, P10, and P28. GFP+ photoreceptors were enriched by FACS (FACSAria; BD Biosciences) (see Fig. 9). RNA was extracted from 1–5 $\times$ 10^5 flow-sorted cells and evaluated by RT-PCR using selected marker genes (see Fig. 10, which is published as supporting information on the PNAS web site). Total RNA (40–60 ng) was used for linear amplification with Ovation Biotin labeling system (Nugen, San Carlos, CA), and 2.75 μg of biotin-labeled fragmented cDNA was hybridized to mouse GeneChips MOE430.2.0 (Affymetrix) having 45,101 probesets (corresponding to >39,000 transcripts and 34,000 annotated mouse genes). Four to six independent samples were used for each time point.

Gene Filtering and Analysis. The "AFFY" package (45) was used to generate "present" and "absent" calls, for every gene at each developmental stage, based on a majority rule over the replicates. Each of the 45,101 probesets was assigned to one of the 32 possible clusters based on its presence/absence pattern across five time points. The 22,611 "present" probesets are henceforth referred to as genes. The Robust Multichip Average method (46) was used for background correction, quantile normalization, and summarization of expression scores. These genes were further subjected to two-stage filtering procedure based on the theory of FDR-CIs (47), as described (26). The FDR-CI *P* value for a given gene is defined as the minimum significance level *q* for which the gene's FDR-CI does not intersect the [-fcmin, fcmin] interval (e.g., fcmin = 1 corresponds to a 2-fold change in log 2 scale). Microarray data in MIAME format (48) has been deposited in the Gene Expression Omnibus database GEO (www.ncbi.nlm.nih.gov/geo).

SOM and Hierarchical Gene Clusterings. The top 1,000 FDR-CI constrained gene profiles were standardized to have mean of 0 and SD of 1 across five time points and clustered by using SOM implemented in Gene Cluster II (36) and hierarchical clustering implemented in CLUSTER and TREEVIEW (49). Euclidean distance was chosen for clustering as the measure of expression profile similarity. For SOM, clusters of similarly expressed genes were projected onto a 2D 2 $\times$ 4 grid, which was selected empirically to capture biologically nonredundant patterns of interest. For hierarchical analysis, clusters were defined by selecting a certain branch length (height) of the dendrogram. Gene Ontology analysis of SOM and hierarchical clusters was performed as described (www.affymetrix.com/analysis/index.affx).

We thank C. Cepko, J. S. Friedman, P. F. Hitchcock, H. Khanna, B. E. Knox, P. Raymond, T. Saunders, and D. L. Turner for stimulating discussions; M. Gillett, D. Molnar, O. Popoola, S. Reske, M. Van Keuren, and D. Wilson for technical assistance; and S. Ferrara for administrative support. This research was supported by grants from the National Institutes of Health (EY11115, EY14259, EY07003, and EY13934), the Foundation Fighting Blindness, Research to Prevent Blindness, and the Elmer and Sylvia Sramek Foundation.

1. Levine, M. & Tjian, R. (2003) *Nature* **424,** 147–151.
2. Brivanlou, A. H. & Darnell, J. E., Jr. (2002) *Science* **295,** 813–818.
3. Ptashne, M. & Gann, A. (2001) *Essays Biochem.* **37,** 1–15.
4. Davidson, E. H., McClay, D. R. & Hood, L. (2003) *Proc. Natl. Acad. Sci. USA* **100,** 1475–1480.
5. Livesey, F. J. & Cepko, C. L. (2001) *Nat. Rev. Neurosci.* **2,** 109–118.
6. Cayouette, M., Barres, B. A. & Raff, M. (2003) *Neuron* **40,** 897–904.
7. Levine, E. M., Fuhrmann, S. & Reh, T. A. (2000) *Cell Mol. Life Sci.* **57,** 224–234.
8. Carter-Dawson, L. D. & LaVail, M. M. (1979) *J. Comp. Neurol.* **188,** 263–272.
9. Young, R. W. (1985) *Anat. Rec.* **212,** 199–205.
10. Young, R. W. (1985) *Brain Res.* **353,** 229–239.
11. Brown, N. L., Patel, S., Brzezinski, J. & Glaser, T. (2001) *Development (Cambridge, U.K.)* **128,** 2497–2508.
12. Hatakeyama, J., Tomita, K., Inoue, T. & Kageyama, R. (2001) *Development (Cambridge, U.K.)* **128,** 1313–1322.
13. Wang, S. W., Kim, B. S., Ding, K., Wang, H., Sun, D., Johnson, R. L., Klein, W. H. & Gan, L. (2001) *Genes Dev.* **15,** 24–29.
14. Cepko, C. L., Austin, C. P., Yang, X., Alexiades, M. & Ezzeddine, D. (1996) *Proc. Natl. Acad. Sci. USA* **93,** 589–595.
15. Molday, R. S. & MacKenzie, D. (1983) *Biochemistry* **22,** 653–660.
16. Cepko, C. (2000) *Nat. Genet.* **24,** 99–100.
17. Morrow, E. M., Belliveau, M. J. & Cepko, C. L. (1998) *J. Neurosci.* **18,** 3738–3748.
18. Swaroop, A., Xu, J. Z., Pawar, H., Jackson, A., Skolnick, C. & Agarwal, N. (1992) *Proc. Natl. Acad. Sci. USA* **89,** 266–270.
19. Swain, P. K., Hicks, D., Mears, A. J., Apel, I. J., Smith, J. E., John, S. K., Hendrickson, A., Milam, A. H. & Swaroop, A. (2001) *J. Biol. Chem.* **276,** 36824–36830.
20. Coolen, M., Sii-Felice, K., Bronchain, O., Mazabraud, A., Bourrat, F., Retaux, S., Felder-Schmittbuhl, M. P., Mazan, S. & Plouhinec, J. L. (2005) *Dev. Genes Evol.* **215,** 327–339.
21. Rehemtulla, A., Warwar, R., Kumar, R., Ji, X., Zack, D. J. & Swaroop, A. (1996) *Proc. Natl. Acad. Sci. USA* **93,** 191–195.
22. Chen, S., Wang, Q. L., Nie, Z., Sun, H., Lennon, G., Copeland, N. G., Gilbert, D. J., Jenkins, N. A. & Zack, D. J. (1997) *Neuron* **19,** 1017–1030.
23. Mitton, K. P., Swain, P. K., Chen, S., Xu, S., Zack, D. J. & Swaroop, A. (2000) *J. Biol. Chem.* **275,** 29794–29799.
24. Lerner, L. E., Gribanova, Y. E., Ji, M., Knox, B. E. & Farber, D. B. (2001) *J. Biol. Chem.* **276,** 34999–35007.
25. Cheng, H., Khanna, H., Oh, E. C., Hicks, D., Mitton, K. P. & Swaroop, A. (2004) *Hum. Mol. Genet.* **13,** 1563–1575.
26. Yoshida, S., Mears, A. J., Friedman, J. S., Carter, T., He, S., Oh, E., Jing, Y., Farjo, R., Fleury, G., Barlow, C., et al. (2004) *Hum. Mol. Genet.* **13,** 1487–1503.
27. Bessant, D. A., Payne, A. M., Mitton, K. P., Wang, Q. L., Swain, P. K., Plant, C., Bird, A. C., Zack, D. J., Swaroop, A. & Bhattacharya, S. S. (1999) *Nat. Genet.* **21,** 355–356.
28. Nishiguchi, K. M., Friedman, J. S., Sandberg, M. A., Swaroop, A., Berson, E. L. & Dryja, T. P. (2004) *Proc. Natl. Acad. Sci. USA* **101,** 17819–17824.
29. Mears, A. J., Kondo, M., Swain, P. K., Takada, Y., Bush, R. A., Saunders, T. L., Sieving, P. A. & Swaroop, A. (2001) *Nat. Genet.* **29,** 447–452.
30. Daniele, L. L., Lillo, C., Lyubarsky, A. L., Nikonov, S. S., Philp, N., Mears, A. J., Swaroop, A., Williams, D. S. & Pugh, E. N., Jr. (2005) *Invest. Ophthalmol. Visual Sci.* **46,** 2156–2167.
31. Blanks, J. C. & Johnson, L. V. (1983) *J. Comp. Neurol.* **221,** 31–41.
32. Akimoto, M., Filippova, E., Gage, P. J., Zhu, X., Craft, C. M. & Swaroop, A. (2004) *Invest. Ophthalmol. Visual Sci.* **45,** 42–47.
33. Sinitsina, V. F. (1971) *Arkh. Anat. Gistol. Embriol.* **61,** 58–67.
34. Szel, A., Lukats, A., Fekete, T., Szepessy, Z. & Rohlich, P. (2000) *J. Opt. Soc. Am. A* **17,** 568–579.
35. Swaroop, A. & Zack, D. J. (2002) *Genome Biol.* **3,** REVIEWS1022.
36. Reich, M., Ohm, K., Angelo, M., Tamayo, P. & Mesirov, J. P. (2004) *Bioinformatics* **20,** 1797–1798.
37. Blackshaw, S., Harpavat, S., Trimarchi, J., Cai, L., Huang, H., Kuo, W. P., Weber, G., Lee, K., Fraioli, R. E., Cho, S. H., *et al.* (2004) *PLoS Biol.* **2,** E247.
38. Mu, X., Zhao, S., Pershad, R., Hsieh, T. F., Scarpa, A., Wang, S. W., White, R. A., Beremand, P. D., Thomas, T. L., Gan, L., *et al.* (2001) *Nucleic Acids Res.* **29,** 4983–4993.
39. Dorrell, M. I., Aguilar, E., Weber, C. & Friedlander, M. (2004) *Invest. Ophthalmol. Visual Sci.* **45,** 1009–1019.
40. Strettoi, E., Mears, A. J. & Swaroop, A. (2004) *J. Neurosci.* **24,** 7576–7582.
41. Ng, L., Hurley, J. B., Dierks, B., Srinivas, M., Salto, C., Vennstrom, B., Reh, T. A. & Forrest, D. (2001) *Nat. Genet.* **27,** 94–98.
42. Okano, T., Kojima, D., Fukada, Y., Shichida, Y. & Yoshizawa, T. (1992) *Proc. Natl. Acad. Sci. USA* **89,** 5932–5936.
43. Yokoyama, S. & Blow, N. S. (2001) *Gene* **276,** 117–125.
44. Arendt, D., Tessmar-Raible, K., Snyman, H., Dorresteijn, A. W. & Wittbrodt, J. (2004) *Science* **306,** 869–871.
45. Gautier, L., Cope, L., Bolstad, B. M. & Irizarry, R. A. (2004) *Bioinformatics* **20,** 307–315.
46. Irizarry, R. A., Hobbs, B., Collin, F., Beazer-Barclay, Y. D., Antonellis, K. J., Scherf, U. & Speed, T. P. (2003) *Biostatistics* **4,** 249–264.
47. Benjamini, Y. & Yekutieli, D. (2005) *J. Am. Stat. Assoc.* **100,** 71–80.
48. Brazma, A., Hingamp, P., Quackenbush, J., Sherlock, G., Spellman, P., Stoeckert, C., Aach, J., Ansorge, W., Ball, C. A., Causton, H. C., *et al.* (2001) *Nat. Genet.* **29,** 365–371.
49. Eisen, M. B., Spellman, P. T., Brown, P. O. & Botstein, D. (1998) *Proc. Natl. Acad. Sci. USA* **95,** 14863–14868.